Author's personal copy

Engineering Fracture Mechanics 76 (2009) 2384–2398

Contents lists available at ScienceDirect

Engineering Fracture Mechanics

journal homepage: www.elsevier.com/locate/engfracmech

Investigation of fatigue crack closure using multiscale image correlation experiments

J. Carroll [a], C. Efstathiou [a], J. Lambros [b,*], H. Sehitoglu [a], B. Hauber [c], S. Spottswood [c], R. Chona [c]

[a] Department of Mechanical Science and Engineering, University of Illinois at Urbana-Champaign, 1206 W. Green Street, Urbana, IL 61801, USA
[b] Department of Aerospace Engineering, University of Illinois at Urbana-Champaign, 104 S. Wright Street, Urbana, IL 61801, USA
[c] Air Force Research Laboratory, AFRL/VASM, 2790 D. Street, Wright-Patterson AFB, OH 45433-7402, USA

ARTICLE INFO

Article history:
Received 12 August 2008
Received in revised form 24 June 2009
Accepted 3 August 2009
Available online 7 August 2009

Keywords:
Digital image correlation
Fatigue crack closure
Fatigue
Crack growth
Titanium

ABSTRACT

Two full-field macroscale methods are introduced for estimating fatigue crack opening levels based on digital image correlation (DIC) displacement measurements near the crack tip. Crack opening levels from these two full-field methods are compared to results from a third (microscale) method that directly measures opening of the crack flanks immediately behind the crack tip using two-point DIC displacement gages. Of the two full-field methods, the first one measures effective stress intensity factors through the displacement field (over a wide region behind and ahead of the crack tip). This method reveals crack opening levels comparable to the limiting values (crack opening levels far from the crack tip) from the third method (microscale). The second full-field method involves a compliance offset measurement based on displacements obtained near the crack tip. This method delivers results comparable to crack tip opening levels from the microscale two-point method. The results of these experiments point to a normalized crack tip opening level of 0.35 for $R \sim 0$ loading in grade 2 titanium. This opening level was found at low and intermediate ΔK levels. It is shown that the second full-field macroscale method indicates crack opening levels comparable to surface crack tip opening levels (corresponding to unzipping of the entire crack). This indicates that effective stress intensity factors determined from full-field displacements could be used to predict crack opening levels.

© 2009 Elsevier Ltd. All rights reserved.

1. Introduction

It is widely accepted that precise knowledge concerning failure mechanisms allows designers to use increasingly aggressive structural designs. The safe life design paradigm is no longer acceptable for many applications since it leads to conservative designs that are too heavy, exhibit poor performance, and/or require excessive maintenance. Modern aviation requirements have necessitated a damage tolerant design approach wherein a structure is designed to withstand a certain amount of damage without failure. Such an approach strongly depends on accurate predictions of fatigue crack growth rates. In the 1960s, Paris and Erdogan [1] and McEvily and Boettner [2] related the fatigue crack growth rate, da/dN to the stress intensity factor range, ΔK, through the Paris relationship:

$$\frac{da}{dN} = C(\Delta K)^m, \tag{1}$$

* Corresponding author.
E-mail address: lambros@uiuc.edu (J. Lambros).

0013-7944/$ - see front matter © 2009 Elsevier Ltd. All rights reserved.
doi:10.1016/j.engfracmech.2009.08.002

Author's personal copy

where C and m are empirical material and loading dependent constants. The advent of the servo-hydraulic load frame allowed McEvily and Boettner [2] to conduct a large number of experiments necessary for validating the Paris relationship (1). The load ratio, R (minimum load divided by maximum load), was also found to have a major effect on crack growth rates.

In the early 1970s, Elber [3,4], discovered the crack closure phenomenon and modified the Paris relationship to use only the portion of the stress intensity range above the crack opening level, ($\Delta K_{eff} = K_{max} - K_{open}$), as follows:

$$\frac{da}{dN} = C(\Delta K_{eff})^m. \tag{2}$$

Using ΔK_{eff} largely eliminated the direct dependence of crack growth rate on the load ratio such that one parameter, ΔK_{eff}, could be used instead of two (K and R), thereby demonstrating that plasticity-induced crack closure was the mechanism responsible for the effect of *load ratio* on crack growth rates. Crack closure acts as a shielding mechanism that reduces the effective stress intensity factor range at the crack tip, thereby decreasing crack growth rates.

Elber [3,4] showed that crack opening would be accompanied by a change in specimen compliance (due to a configuration change when the crack opens). He found the load level corresponding to this compliance change by using a displacement gage 2 mm behind the crack tip to measure the relative displacement of the crack flanks. Since Elber's discovery, several other techniques have been developed for measuring crack closure. Some researchers use visual observations and/or replica techniques to determine closure levels [5,6]. Other methods for measuring crack closure such as the electrical potential drop method, ultrasonic/acoustic methods, and the eddy current method have been used with limited success. Schijve [7] provides a brief comparison of these and other methods.

Despite these newer techniques, using displacement gages to detect a compliance change remains the most popular method for finding crack closure levels. Back face strain gages, crack mouth gages, or clip gages anywhere on the specimen can be used [8]. Following the pioneering work of Elber [3,4], displacement gages are typically placed across the crack faces within a few millimeters of the crack tip. These displacement gages need not physically contact the crack faces. Often, non-contact displacement gages make it relatively easy to place many gages along the crack line so that the variation in local crack opening levels with distance from the crack tip can be observed. Macha et al. [9] used laser interferometric displacement gages, which track indentation marks near the crack flanks, to measure local crack opening displacement along the crack length. In a similar manner, Digital Image Correlation (DIC) displacement gages were introduced by Riddell et al. [10] and Sutton et al. [11] (for details on the technique of digital image correlation, the reader is referred to references [12,13]). These displacement gages use DIC to track two subsets, one on each crack flank, to measure the crack opening displacement. As the crack opens, the subsets move apart from each other and the crack opening displacement at the gage location is measured as the relative motion between the two subsets. Similar DIC displacement gages are used in this work. Using displacement gages on the crack flanks allows both *local* and *crack tip* opening levels to be determined.

Although crack opening occurs gradually from the crack mouth to the crack tip, a single opening level must be defined to obtain a single value for ΔK_{eff}. The crack tip opening level is typically used since it is thought that crack growth cannot occur until the crack is fully open. However, it is difficult to precisely identify the crack tip opening level due to scatter in experimental measurements and the fact that crack opening is a continuous process. This difficulty has spurred several analysis techniques of the load versus displacement curve to obtain ΔK_{eff} [14–16]. Donald and Paris [14] give a review of seven of these analysis methods including the partial closure model of Paris et al. [15]. Predictions of crack growth rates based on each of these models are compared by Donald and Paris [14]. The partial closure model of Paris et al. [15] appears to give slightly better results than other models under the circumstances considered by Donald and Paris, but with the amount of scatter in the measurements, a clearly superior model has yet to emerge.

Adding to the ambiguity is the fact that crack closure is three-dimensional in nature because of constraint condition variations [17] (i.e., plane stress on the surface versus plane strain in the specimen's interior). Budiansky and Hutchinson provided one of the first analytical studies of crack closure [18], and countless numerical models of the crack closure process have followed [17,19–21]. Numerical models have also been influential in the debate over the existence of plasticity-induced crack closure under plane strain conditions [20,21]. The three-dimensional aspect of crack closure was also studied by Riddell et al. [10]. By comparing a finite element analysis of crack closure to rate-calculated opening loads, the researchers showed that, for their specimens, crack tip closure levels on the interior of the specimen (which are lower than those on the surface of the specimen due to constraint effects) dominated the crack closure effect on fatigue crack growth. They argued that surface crack closure measurements at the crack tip overestimate the crack closure effect.

Further complicating the study of crack closure is the existence of multiple closure mechanisms. These mechanisms include plasticity-, roughness-, phase transformation-, viscous fluid-, and oxidation-induced crack closure [22]. Measured crack closure levels are generally due to a combination of mechanisms (most commonly plasticity- and roughness-induced crack closure). Since the effects of different closure mechanisms could not be delineated in this work, the cited closure levels are possibly a combination of plasticity-induced, roughness-induced, and oxidation-induced crack closure. However, plasticity is likely the primary closure mechanism in these experiments since, as will be seen later, very little shear motion of the crack faces is observed here.

In summary, it is clear that crack closure is an extremely important effect that needs to be accounted for to predict crack growth rates accurately, but it is highly complicated in nature and dependent on the scale of observation – as the crack tip is approached, different amounts of local closure are observed. The objective of this work is to combine some of the techniques

Author's personal copy

that have individually been used in the past in a multiscale framework that will allow experimentally linking measures of crack closure at locations close to and far from the crack tip. Specifically, full-field displacement measurements at the macroscale (order of mm) can be used to calculate the effective stress intensity factor range and, in turn, calculate closure levels. At the microscale, (order of μm) non-contact displacement gages can be used to quantify crack tip closure. The DIC technique, which does not possess an inherent length scale, is highly suitable for such multiscale experimentation and will facilitate direct linking between the scales. Section 2 of this paper describes the experimental approach used. The subsequent section provides results of the microscale experiments followed by the macroscale results and finally a link between the two scales.

2. Experimental procedure

Edge-notched tension specimens were cut from a plate of grade 2 (commercially pure) titanium with electrical discharge machining (EDM); a 0.30 mm EDM wire was used to machine the notch (see Fig. 1a for specimen geometry). From both ultrasonic testing and simple tension tests, the modulus of elasticity and Poisson's ratio were found to be 109 GPa and 0.33, respectively. The yield stress of 400 MPa was also determined from simple tension tests. Microscopy on etched specimens indicated a grain size of roughly 10 μm. By testing specimens of different orientations, the properties of elastic modulus and Poisson's ratio were found to be isotropic. Each specimen was rough polished using abrasive paper up to 800 grit. The natural texture of the specimen surface after rough polishing provided a suitable speckle pattern for using DIC; therefore, the specimens were not painted. See Fig. 1b for a comparison of the resulting speckle patterns at each magnification. Although the speckle pattern appears more suitable for DIC at some magnifications than others, correlation accuracy was found to be acceptable at all magnifications.

Specimens were fatigued at rates between 2 and 8 Hz to initiate and grow a crack from the EDM notch tip at constant load amplitude and a load ratio of roughly zero. Consequently, the stress intensity factor slowly increased throughout the crack growth process. The servo-hydraulic load frame was controlled by a computer program that allowed images to be associated with their corresponding load levels (measured using a 100 kN load cell). After a period of crack growth, (see Table 1 for the number of crack growth cycles for each experiment) the fatigue loading was stopped and several "measurement" cycles were applied to the specimen at a much slower rate of 240 s per cycle. This slower rate allowed 120 images to be captured throughout the loading cycle so that a typical fatigue cycle could be studied in detail. Except for frequency, measurement cycles were equivalent to the last high frequency cycle. In this work, crack growth rates were on the order of 10^{-5} mm/cycle. If the threshold crack growth rate corresponds to approximately one Burger's vector per cycle (2×10^{-7} mm/cycle), then these experiments are two orders of magnitude above the threshold crack growth rate.

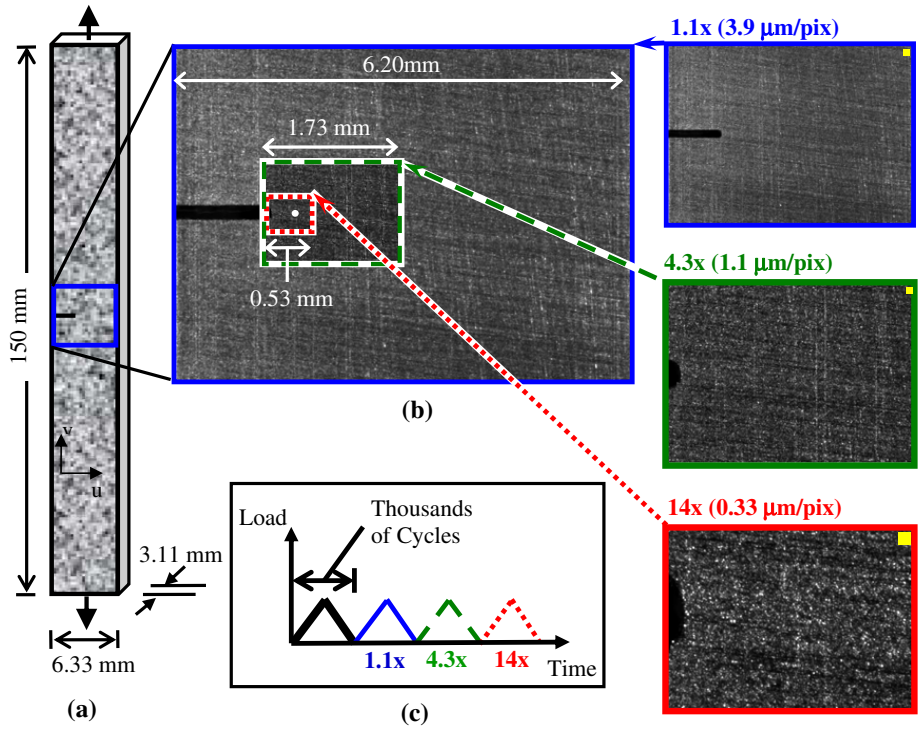

Fig. 1. (a) Specimen geometry and dimensions. (b) Field of view and resolution at each magnification level. The crack tip is shown as a white dot in the center set of images. Images are shown at the same size at the right to allow comparisons of speckle patterns. DIC subset sizes are shown by a square in the top right corner of each image. (c) Typical loading history. Data gathered from each magnification level was from a different cycle.

Author's personal copy

Table 1
Details of each experiment. Load ratio R is P_{min}/P_{max}.

Experiment	K_{max} (MPa$\sqrt{}$m)	R	Width (mm)	Thickness (mm)	Notch length, c (mm)	Crack length, l (mm)	l/c	Crack growth cycles
Low K	9.7	0.05	6.33	3.11	0.980	0.680	0.69	24,894
Medium K	15.4	0.05	6.34	3.10	0.969	0.906	0.93	15,752
High K	18.9	0	6.30	3.12	1.374	0.351	0.26	2,753

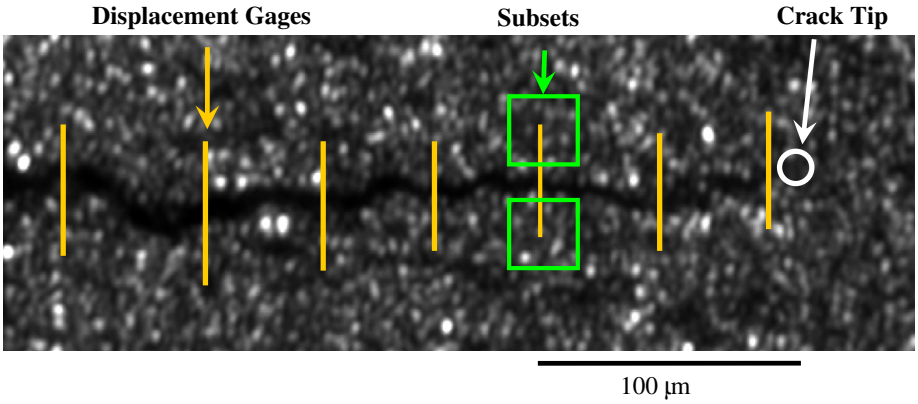

Fig. 2. Illustration of seven DIC displacement gages across open crack faces imaged at 14×. Each gage consists of two subsets—one on each of the crack flanks.

A digital camera with a resolution of 1600 by 1200 pixels was used to capture images throughout measurement cycles. Optical magnifications from 1.1× to 28× (3.8 to 0.17 μm/pixel, respectively) were achieved with an adjustable lens with a 12× magnification range and a 2× adapter tube. Each measurement cycle was viewed with a different magnification as illustrated in Fig. 1c. In all, three magnifications were used in measurement cycles: two "macroscopic" magnifications of 1.1× and 4.3× (3.8 and 1.1 μm/pixel, respectively) and one microscopic magnification of 14× (0.33 μm/pixel) as illustrated in Fig. 1b. Using multiple cameras would allow images to be captured at multiple magnifications simultaneously within a single cycle [23]. However, for simplicity, one camera was used with a different measurement cycle for each magnification (see Fig. 1c). The scales cited in Fig. 1b are approximate since many cycles were run at each magnification. The exact scale used in calculations was determined for each measurement cycle individually. Fig. 1b also compares the speckle pattern at each magnification.

DIC was performed on images from each of the measurement cycles using a commercially available image correlation program. The first image in the measurement cycle (at minimum load) was used as the reference image, and terms up to first order displacement gradients were used in all correlations. For loading cycles observed at the microscopic magnification (14×), DIC displacement gages spanning the crack faces [10,11] were used. Several gages were placed along the crack length as shown in Fig. 2, which illustrates a 14× image of a fully open crack at peak load. Subset sizes of 81 by 81 pixels were used corresponding to a gage width of 27 μm. A typical gage length was 40 μm, and gages used in this work were placed from 10 μm *ahead* of the crack tip to 700 μm *behind* the crack tip. For both of the macroscopic loading cycles (1.1× and 4.3×), DIC was used to obtain full-field displacements for each image throughout the cycle. Correlations were performed using a subset size of 41 by 41 pixels and a spacing of 15 pixels between subset centers.

Each measurement cycle was observed at a different magnification (i.e. the 1.1× images were captured over a different cycle than the 4.3× or the 14× images). All measurement cycles were within eight cycles of each other (some cycles are not discussed in this paper). From our measurements of crack growth rates, the amount of crack growth throughout eight cycles was less than one pixel at 14× magnification and no crack growth was observed during this small number of cycles. Therefore, the data from each measurement cycle are considered to be from equivalent cycles and are assumed representative of previous fatigue cycles. After the measurement cycles, the specimen was loaded to peak load and photographed at a very high magnification of 28× (0.17 μm/pixel). DIC was not performed on these images, rather the peak load images were simply observed to identify the crack tip location accurately. Identifying the crack tip on a speckled surface can be difficult, and without an accurate estimate of the crack tip location, the error in these analyses becomes unacceptably large.

To investigate the effects of peak stress intensity factor on crack closure, three experiments were performed, each with a separate specimen, using the aforementioned procedure. The maximum stress intensity factors during measurement cycles for these experiments were 9.7, 15.4, and 18.9 MPa$\sqrt{}$m. In each case, precracking was performed under load control at the same load level as the fatigue cycles imaged using DIC. These three experiments will be referred to as the "low K", "medium K", and "high K" experiments, respectively. Details of each experiment such as specimen geometry, loading specifications, and the number of cycles of fatigue crack growth can be found in Table 1.

Author's personal copy

3. Results and discussion

3.1. Microscale measurements (14×)

At the microscopic magnification, DIC displacement gages were used to measure crack opening displacements along the crack length. Gage displacement is defined here as the relative vertical displacement of the gage's two subsets ignoring in-plane shearing displacements. Shearing displacements were found to be extremely small (less than one pixel), were about two orders of magnitude less than opening displacements, and were in fact near the lower resolution limit of DIC. A load versus displacement plot, such as the one shown in Fig. 3, was created for each DIC displacement gage. Each data point in Fig. 3 represents gage displacement at a specified load level (one image per point) with the loading portion of the cycle represented by circles and the unloading portion by triangles.

Elber noted that a change in slope of the load versus displacement curve is a change in specimen compliance. He also showed that this compliance change must be due to crack opening and not other factors such as plasticity. When the specimen is first loaded, the gage displacement remains nearly zero indicating the crack is closed at this gage location. Any gage displacement in this low-load region is due to material strain between the gage points, not crack opening. As the crack opens at the gage location, the gage displacement begins to increase at a significant rate (this is the load denoted by the "local opening" arrow in Fig. 3). As the crack opens ahead of the gage, a gradual compliance change occurs until the crack is fully open up to the crack tip (see "crack tip opening" in Fig. 3). Because the crack is fully open, loading the specimen further results in a linear relationship between load and gage displacement (no further compliance change), at least before large scale plasticity effects begin.

The *local* crack opening level is identified by the load at which the gage displacement begins to increase significantly. This load level is computed by fitting a straight line to the upper linear portion of the loading curve in Fig. 3 and visually determining where the gage displacement first deviates from this line. The *crack tip opening level* can also be identified from the load versus displacement curve, but is more difficult to do so since it usually induces a more gradual compliance change. The ASTM compliance offset method (described in detail later in this section) is used to identify the end of this gradual compliance change. The local closing load can be determined similarly to the local opening load; however, the crack tip closure load cannot be determined from this method since reverse plasticity affects the apparent compliance change upon unloading.

Load versus displacement curves for several gages along the crack length illustrate how local crack opening loads vary with position. Fig. 4a–c shows load versus gage displacement curves for three different gages (in the low K experiment). These three gages are located (a) 665 μm (b) 236 μm and (c) 64 μm behind the crack tip. Note that the stiffness increases and the local crack opening and closure levels increase as the crack tip is approached. This behavior is expected since cracks generally open first at the mouth and last at the crack tip.

Since several subsets were placed along the crack flanks, a visualization of the crack profile can be created by measuring the vertical displacement of each individual subset (not the gage displacement). Vertical subset displacements are plotted in Fig. 5 (with rigid translation subtracted) to create crack profile plots at four different load levels within a typical fatigue cycle. This particular cycle is for the low K experiment, and the load level is shown as a percentage of peak load. Fig. 5 indicates that the majority of the crack (beyond 150 μm *behind* the crack tip) appears open by 18% of the peak load, and the entire crack is fully open, to the extent imaged at the magnification used here, by 31% of the peak load. The single gage on the right is about

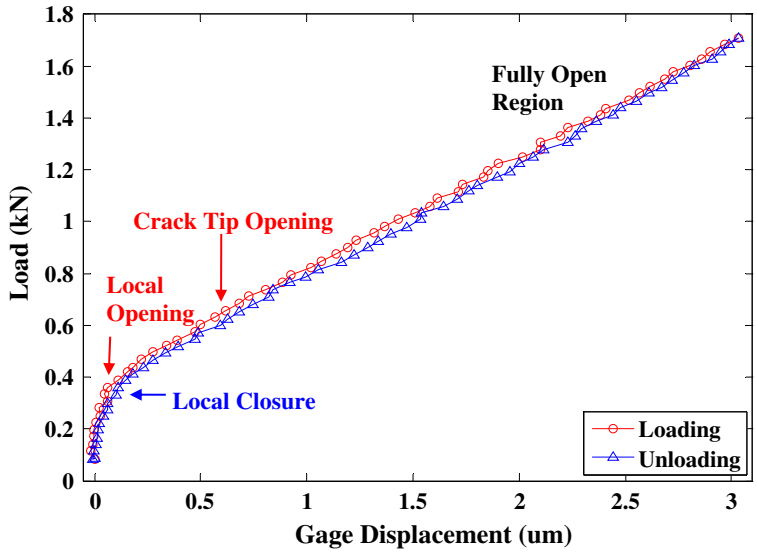

Fig. 3. Load versus displacement curve for a typical DIC displacement gage (Low K). Local opening levels are defined by the sharp knee in the curve while the compliance offset method is required to detect the more gradual compliance change caused by crack tip opening. Local closure values are found from the sharp knee of the unloading portion of the curve.

Author's personal copy

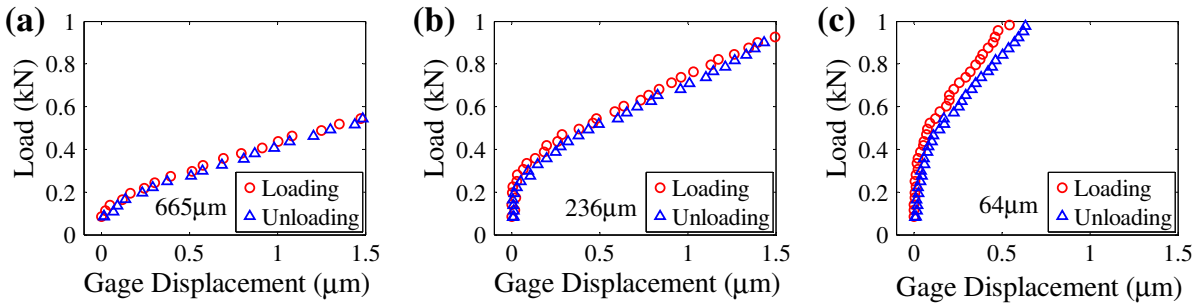

Fig. 4. Load versus displacement curves for: (a) 665 μm, (b) 236 μm, and (c) 64 μm behind the crack tip. (Data from low *K* experiment).

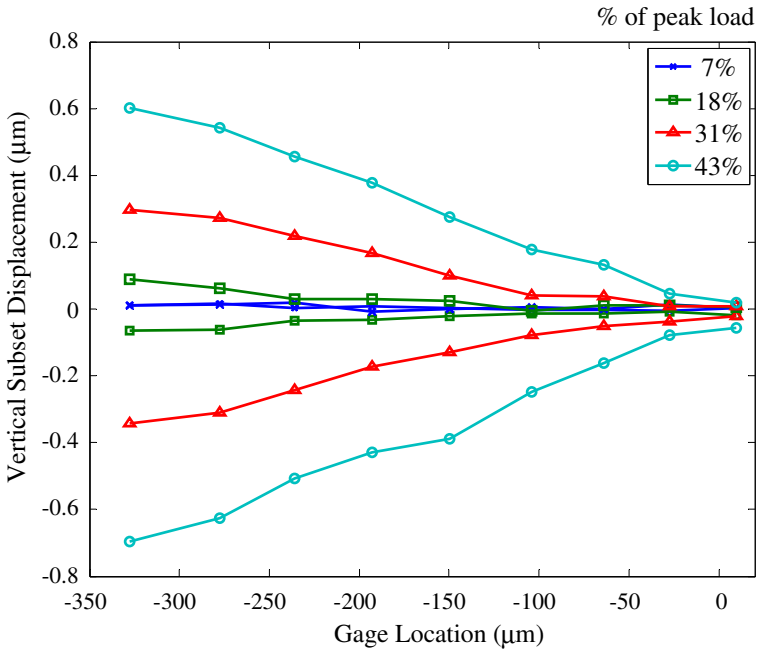

Fig. 5. Crack profiles constructed from vertical subset displacement measurements at 14× for several load levels of the low *K* experiment. The crack tip is located at 0 μm. Note that the single gage *ahead* of the crack tip never appears open.

10 μm *ahead* of the crack tip and, as expected, never appears open. These profile plots give a visual representation of the crack opening process, but it is important to note that the visual and mechanical crack tip opening do not necessarily coincide. It is the mechanical opening, as measured in Fig. 3, when the crack faces become truly traction free, that determines ΔK_{eff}.

While local crack opening measurements do provide insight as to the mechanics of crack opening and closure, an unambiguous measure of the crack opening level at the tip is ultimately necessary for the modified Paris relationship (2). However, detecting the compliance change related to the crack tip opening level is more difficult than detecting the local opening level since the compliance change associated with crack tip opening is less abrupt (refer to Fig. 3). To detect this more gradual compliance change, the compliance offset method outlined in appendix X2 of ASTM standard E647 [24] was followed. For a detailed description of the procedure, the reader is referred to the ASTM standard; the method is briefly outlined below to provide specifics. A line is fit to the top linear portion of the unloading curve (the top 25% of the curve was used here) using least squares regression, and the inverse of this slope is defined as the compliance of the specimen with the fully open crack. The unloading slope is used in order to avoid any plasticity effects associated with loading. In a similar manner, lines are fit to fractions of the loading portion of the curve (in this case, a fit was made to 10% of the load range at intervals of 5% so that each line fit overlapped by 5% of the load range). The compliance at each of these load levels is found and compared to the unloading compliance. The load at which the compliance difference exceeds 4% is defined as the crack tip opening level.

Values of local and crack tip opening loads are plotted against gage position in Fig. 6. The horizontal axis represents the distance behind the crack tip while the vertical axis represents the opening or closure load (P) normalized by the peak load (P_{max}) expressed as a percentage. These values were calculated from the results of DIC displacement gages in the low *K* experiment using the techniques outlined above. Local crack opening levels are shown as squares while crack tip opening levels calculated from the ASTM compliance offset method are shown as crosses in Fig. 6. Crack tip opening levels are expected to

Author's personal copy

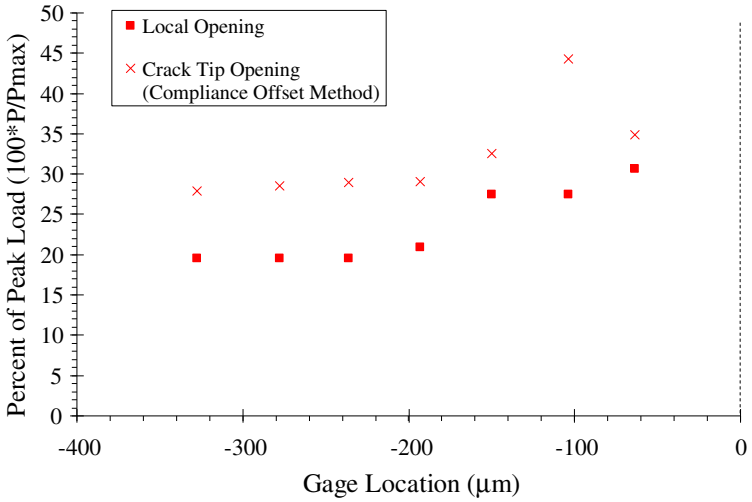

Fig. 6. Local crack opening levels and crack tip opening levels (determined from the compliance offset method) determined from load versus displacement curves from several gages. The horizontal axis represents gage distance behind the crack tip. The vertical axis represents the percentage of the opening (or closure) load, P, divided by the peak load, P_{max}.

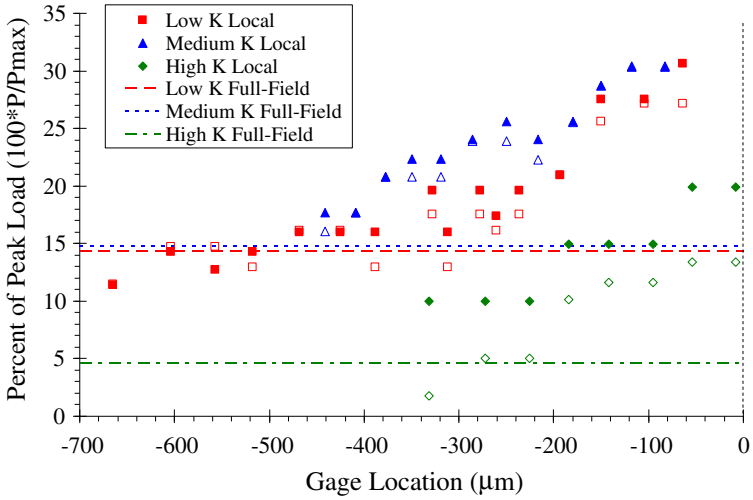

Fig. 7. Local opening and closure levels from the microscale measurements (points) and macroscale measurements (lines) for three different K_{max} values. 0 μm denotes the crack tip location. Symbols indicate displacement gage measurements while lines indicate measurements from the full-field effective K method. The horizontal axis represents gage distance behind the crack tip. The vertical axis represents the percentage of the opening (or closure) load, P, divided by the peak load, P_{max}.

be independent of gage location [3,4], but a slight increasing trend is observed as the crack tip is approached (in both local and crack tip opening loads). However, the amount of difference between load levels is roughly equal to the noise in experimental measurements. In both methods, the opening levels for gages closest to the crack tip (within 150 μm) are slightly higher than those further behind the tip. However, it is suspected that these measurements are less reliable because this close to the crack tip, plasticity effects may exist even at low loads. Also, the higher opening levels near the crack tip could be due to three-dimensional aspects of crack closure. For conciseness, comparisons of local and crack tip opening levels for the medium and high K experiments have been omitted, but they exhibit behavior similar to Fig. 6.

Local crack opening and closure values determined from DIC displacement gages for all three load levels are presented in Fig. 7. The low, medium, and high K experiments are shown as squares, triangles, and diamonds, respectively. Filled symbols represent opening levels and empty symbols represent closure levels so that each pair of filled and empty symbols represents one displacement gage. Note that the data from the low K experiment cover a larger distance behind the crack tip because two measurement cycles were performed at a magnification of 14× for the low K experiment: one with the imaged area near the crack tip, and a second with the imaged area behind the crack tip by several hundred micrometers.

In agreement with Macha et al. [9] and Riddell et al. [10], the local crack opening (and closure) levels for the low K experiment exhibit two regions. The first region is far behind the crack tip (between 350 and 700 μm behind the tip) where closure levels remain constant. This implies that a large portion of the crack opens at roughly 16% of the peak load. This value agrees with estimates from the crack profile plot of Fig. 5 where the majority of the crack appeared open by 18% of the peak load.

Author's personal copy

The second region of crack opening is near the crack tip (within 350 μm) where closure levels increase as the crack tip is approached. If local crack opening levels are extrapolated to the crack tip location, they can provide an estimate of the crack *tip* opening level. Extrapolating local low K opening values provides a crack tip opening estimate of 35% of the peak load. This value is in agreement with crack profile observations in Fig. 5 (31%) and with the crack tip opening level calculated from the ASTM compliance offset method (Fig. 6) within experimental error.

By extrapolating local crack opening measurements to the crack tip for all three experiments, opening levels at the crack tip are 35%, 34%, and 21% for the low, medium, and high K experiments, respectively. Although there is some uncertainty in these estimates, these values are reasonable estimates of the crack tip opening level on the specimen surface. Limited crack closure data on grade 2 titanium exists with which to compare. However, Takao et al. [26] used the electrical potential drop method and replica techniques on grade 2 titanium to obtain crack closure levels between 27% and 42% ($R = 0$). Measurements from gages closest to the crack tip for the low and medium K experiments are within this range. Measurements from the high K experiment are lower due to the short crack effect explained below.

In Fig. 7, it is clear that displacement gage measurements from the low and medium K experiments are close to one another. Therefore, no conclusions can be drawn concerning the effect of K_{max} on crack opening/closure levels as described in the literature [25]. By observing Fig. 7, it is evident that the opening/closure levels for the high K experiment are below the low and medium K experiment values. This is because the high K experiment has a lower crack-to-notch ratio, l/c (see Table 1). Since the notch surfaces never come into contact, only the fatigue crack contributes to the crack closure phenomenon. With a shorter fatigue crack in the high K experiment, there is less residually stressed material that contributes to crack closure; hence, the high K specimen exhibits lower closure levels. The effect of crack length on crack closure levels was previously observed by Sehitoglu [6].

3.2. Macroscale measurements (1.1× and 4.3×)

In the macroscale experiments, full-field displacements were obtained from DIC. Contour plots of v-displacements (perpendicular to the crack line) were created for each image. As an example, Fig. 8 shows peak load v-displacements in the high K experiment. The origin is placed at the crack tip, and a positive displacement contour means material moved upwards (rigid motion has been subtracted from these plots using the KT regression discussed later). Fig. 8a shows the v-displacement field measured at a magnification of 1.1× while Fig. 8b shows results from the 4.3× field of view, measured independently during two consecutive cycles. The black rectangle in Fig. 8a represents the area shown in Fig. 8b.

Asymptotic theoretical solutions exist for full-field displacements near a crack tip. The stress intensity factor for a single edge-notched tension specimen can be theoretically calculated from continuum mechanics assuming two-dimensional linear elasticity given the load and specimen geometry by

$$K = F\sigma\sqrt{\pi a}, \tag{3}$$

where σ is the nominal stress and a is the crack length. F is given by

$$F = 0.265(1-\alpha)^4 + \frac{0.857 + 0.265\alpha}{(1-\alpha)^{3/2}}, \tag{4}$$

with α being the ratio of crack length to the specimen width [27]. This calculation will be referred to as the "load-based stress intensity factor." Peak stress intensity factors of 9.7, 15.4, and 18.9 MPa$\sqrt{}$m that were cited earlier to classify the low, medium, and high K experiments were calculated through (3) and (4).

To determine what stress intensity factor the specimen actually experiences, which could be different than the theoretical load-based stress intensity factor primarily due to crack closure, a least squares regression was performed on the DIC

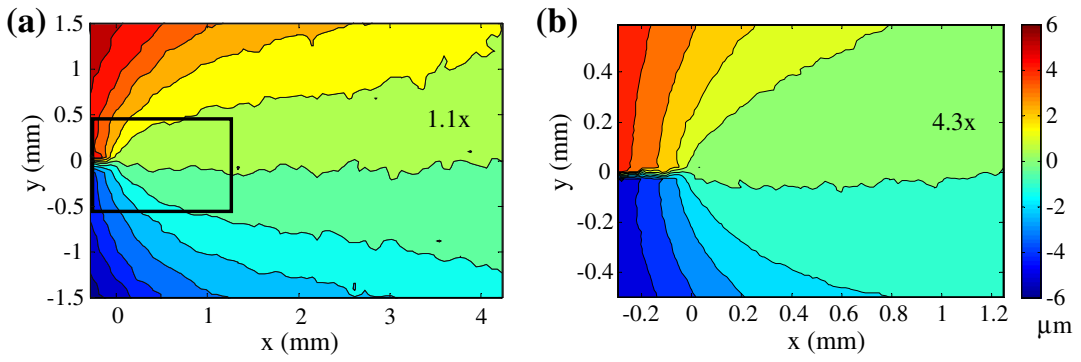

Fig. 8. DIC measured v-displacement field near the crack tip for macroscale images (high K experiment). Rigid motion has been subtracted from these plots for clarity. The black rectangle in: (a), the 1.1× experiment, represents the area shown in (b), measured independently in the 4.3× experiment.

Author's personal copy

measured v-displacements (v) (Fig. 8). Initially, three parameters were used in the regression: stress intensity factor (K), rigid rotation (A), and rigid translation (B) as given by

$$v = \frac{K_I}{\mu}\sqrt{\frac{r}{2\pi}}\sin\left(\frac{\theta}{2}\right)\left[\frac{1}{2}(\kappa+1) - \cos\left(\frac{\theta}{2}\right)\right] + Ar\cos(\theta) + B, \tag{5}$$

where r is the distance from the crack tip, θ is the angle from the crack line ahead of the tip, μ is the shear modulus, and κ is given by:

$$\kappa = \frac{3-\nu}{1+\nu} \tag{6}$$

for plane stress (where ν is Poisson's ratio). This regression is referred to as the K-only regression as it accounts for the contribution to displacement of only the most singular term in the asymptotic expansion for stresses [28].

To determine how well the regression function matches experimental data, Fig. 9a compares DIC measured v-displacements (solid contours) with those calculated from the K-only regression (dotted contours) with the origin placed at the crack tip. For reference, since (5) represents an elastic result, the plane stress Von-Mises plastic zone estimate calculated using the regression K value is shown as a single thick solid contour. As seen in Fig. 9a, the agreement between experimental and regression contours is poor at large distances from the crack tip because the K-only model is an asymptotic solution to the elastic crack problem. As the distance from the crack tip decreases, agreement between experiments and K-only regression (5) improves.

The second term in the Williams expansion for stresses [28] is the T-stress term. As the distance from the crack tip increases, higher order terms (mainly T-stress) have increasing influence over displacements. To account for the T-stress and its effects at larger distances, a second regression was performed. This regression, called the KT regression, includes a parameter for T-stress (T) in addition to the other three parameters used in (5). The KT regression uses v-displacements given by:

$$v = \frac{K_I}{\mu}\sqrt{\frac{r}{2\pi}}\sin\left(\frac{\theta}{2}\right)\left[\frac{1}{2}(\kappa+1) - \cos\left(\frac{\theta}{2}\right)\right] - \frac{1}{2\mu}\left(\frac{\nu}{1+\nu}\right)Tr\sin(\theta) + Ar\cos(\theta) + B. \tag{7}$$

Note that in (7) both the K and the rigid rotation terms apply for the assumption of small displacement gradients. For finite rotations a term involving $Ar\sin(\theta)$, which for regression purposes is the same as the T-stress term in (7), should also be included [29]. In that case the contribution of rigid rotation would be combined with the value of T-stress obtained from the regression, and a second procedure would have to be followed to separate the two [29]. However, by the authors' analysis, the rigid rotation has been found to significantly contribute to the T-stress term only if the rigid rotation (coefficient A in (7)) exceeds 0.5°. In the present effort, the calculated rotation never exceeds 10^{-4}°. Therefore in all cases discussed subsequently, the values of K, T, A, and B used are those fitted directly to the displacement field of (7).

For the low K experiment, the value of T calculated from the 1.1× KT regression varies linearly with load and has a peak value of −94 MPa. The ratio of T to far-field stress remains relatively constant around −0.98 ± 0.17 and is larger than the analytically calculated value of −0.7 found in the literature [30]. For the medium and high K experiments, the T-stress results are similar but show more scatter.

Contours of v-displacement for the KT regression are plotted in Fig. 9b. A comparison with Fig. 9a reveals the effects of including the T-stress parameter: experimental and regression contours match up better over the entire region surrounding the crack tip. Fig. 10a and b shows the same contour comparisons but using the 4.3× experimental results. At this higher magnification closer to the crack tip, displacements are dominated by the K term and the inclusion of the T-stress has little impact on the shape of the regression contours. The K-only regression agrees well with experimental contours and the values

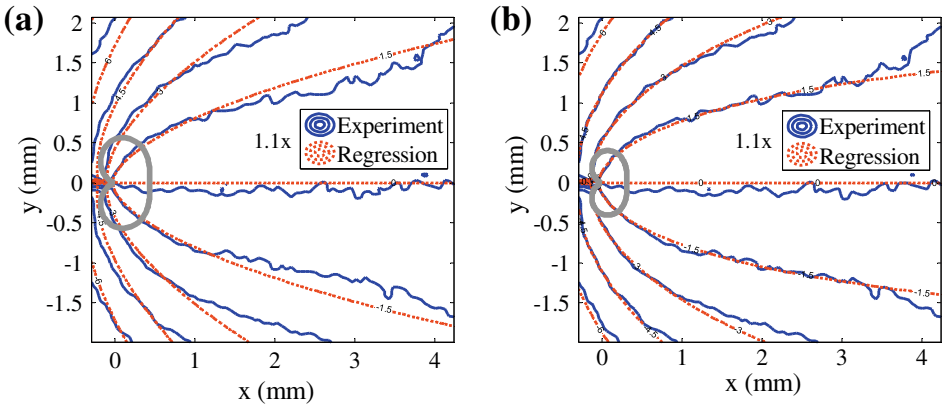

Fig. 9. Comparison of experimentally measured and regression v-displacement contours for: (a) K-only regression and (b) KT regression. The thick solid gray contour represents the approximate Von-Mises plastic zone size. Magnification is 1.1× and contours are spaced by 1.5 μm.

Author's personal copy

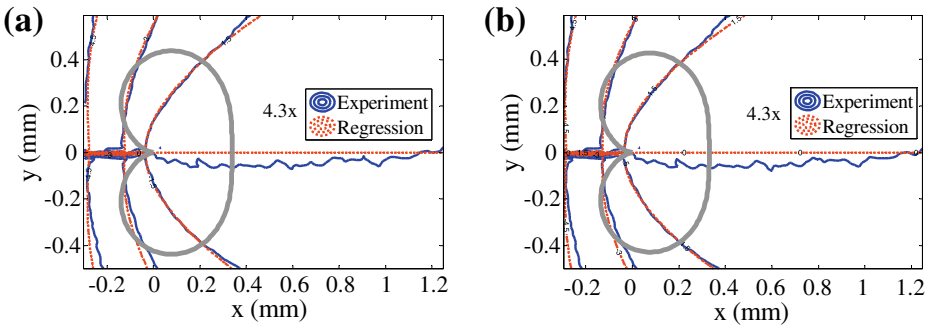

Fig. 10. Comparison of experimentally measured and regression v-displacement contours for: (a) K-only regression and (b) KT regression. The thick solid shape represents the approximate Von-Mises plastic zone size. Magnification is 4.3× and contours are spaced by 1.5 μm.

obtained from both regression methods are the same in this case. However, because the KT regression provides more accurate K values and a better fit to experimental data at all magnifications, the KT regression was used for the results shown in this paper. Terms higher than T-stress were not included because they were found to have negligible effects on regression contours and K values and because their physical significance is questionable. Note that in Fig. 10 the size of the Von-Mises plastic zone contour is a significant portion of the field of view. However, this is only a rough *estimate* of the plastic zone size since it does not include redistribution of the plastic stress. The good agreement of experiments with the elastic KT solutions for stresses could be evidence that the true plastic zone size is smaller than the Von-Mises estimate.

Several researchers [31,32] have performed regressions to obtain stress intensity factors; however, they did not perform such regressions in crack closure situations. Since the reference DIC image is taken at the minimum load of each measurement cycle (not at zero load because the load ratio is above zero), the regression K value is actually the *effective change in stress intensity factor* (not simply the stress intensity factor) at each load. The effective change in stress intensity factor calculated from the KT regression will be referred to as ΔK_r. Results of ΔK_r are plotted against load throughout a typical loading cycle in Fig. 11a as triangles. The load-based theoretical stress intensity factor, K_{theor}, is also shown in Fig. 11a as a straight line passing through the origin. The experimental measurements lag behind the theoretical solution since they exhibit a region at low loading during which the effective stress intensity factor remains nearly zero. This is reminiscent of the response of individual displacement gages in the microscopic experiments, which showed little displacement with initial loading. The curve in Fig. 11b, which is the transpose of Fig. 11a, has a similar shape to the curve in Fig. 3 (load versus gage displacement). The similarity between these plots is due to the fact that ΔK_r is calculated through measurements of the displacement field. When the crack is closed, displacements change very little and the effective stress intensity factor remains near zero. Therefore, the curvature at the beginning of the ΔK_r curve is an indication of crack closure. Once the crack is completely open, ΔK_r increases linearly with load.

The effective stress intensity range, ΔK_{eff}, used in the modified Paris relationship (2) is ideally just the maximum value of ΔK_r. However, a small amount of error in identifying the crack tip can have a pronounced effect on the slope of the linear portion of ΔK_r so that taking the maximum value of ΔK_r can have significant uncertainty. To demonstrate this effect, a KT regression was performed using a bad estimate of crack tip location that was 35 μm behind the identified crack tip (a typical misidentification level). The results of this regression are shown in Fig. 11a. Lines were fit to the top half of the ΔK_r data for both cases of a correctly and an incorrectly identfied crack tip. The slope corresponding to the correctly identified tip is noticeably closer to theory than the slope for the badly estimated crack tip data.

In order to obtain results that are more reliable and in order to compare these measurements to displacement gage crack closure measurements made earlier at the microscale, crack opening/closure levels are calculated from ΔK_r as follows. Elber [3,4] defined the effective stress intensity range, ΔK_{eff} as the difference in the peak stress intensity factor, K_{max}, and the opening stress intensity factor such that

$$\Delta K_{eff} = K_{max} - K_{open}. \tag{8}$$

Since the crack is fully open throughout the linear portion of the ΔK_r versus load curve, the opening level can similarly be calculated at any load by the instantaneous difference in the load-based theoretical stress intensity factor and the change in stress intensity factor ΔK_r as follows:

$$K_{open} = K_{theor} - \Delta K_r. \tag{9}$$

It is posited that K_{theor} is the stress intensity factor that would be experienced by the specimen if closure effects were not present. The slope of the linear portion of the ΔK_r curve does not necessarily match the slope of the K_{theor} due to crack tip identification problems leading to a different calculated opening level value depending on the load at which it is calculated. Since this situation is only an artifact of the difficulty of crack tip identification, the opening stress intensity factor, K_{open}, was instead calculated by taking the difference between K_{theor} and a line of the same slope fitted to the linear (fully open) portion of the ΔK_r experimental results as shown in Fig. 11a. The crack opening level can then be compared to

Author's personal copy

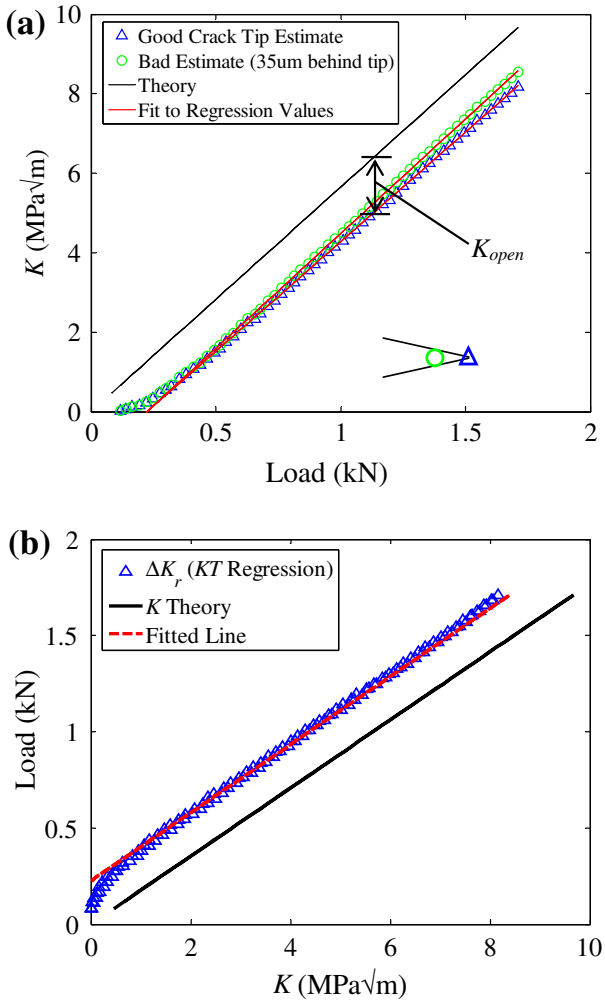

Fig. 11. (a) Finding K_{open} from full-field measurements. Since the value of K obtained from regression is the effective change in stress intensity factor, the opening stress intensity factor can be calculated by the difference between theoretical and regression values. Regression values are shown as triangles while the circles show the effect of making a bad guess for the crack tip location. The fit to each set of regression data illustrates that the main effect of a bad crack tip guess is a change in slope of the data. (b) The transpose of Fig. 10a illustrating the closure effect through a global specimen compliance change.

displacement gage values by dividing K_{open} by the maximum stress intensity factor from theory, K_{max}. This method of finding crack closure levels will be referred to as the "*full-field effective K*" method.

Fig. 12 collects the ΔK_r results for each of the low, medium and high K experiments at the two different macroscale magnifications (1.1× and 4.3×), as available. A few points may be observed from this figure. First, the low and medium K experiments have regression values further below theory than the high K values, indicating less closure in the high K experiments. This is consistent with displacement gage observations (Fig. 7) that the high K experiment had lower closure levels. Second, the high K regression data also show some hysteresis; this could be an indication of notch tip plasticity effects due to a very short fatigue crack and high loads. Third, the medium K regression data appear to be at a slightly different slope than the K values predicted by theory. As mentioned above, this effect is due to measurement error in identifying the crack tip. Identification of the crack tip is done at a magnification of 28×, but there is still some error in this measurement. The crack is not generally shorter than these measurements, but it could be up to 35 μm longer depending on how much of the crack is obscured by the speckle pattern. However, the averaging approach described earlier for computing K_{open} from such macroscopic results is more robust to crack tip position errors. Fourth, as Fig. 12a and c demonstrate, magnification level is shown to have negligible effect on stress intensity factor values, as long as a KT regression is used, although results from 4.3× magnification have less noise than results from 1.1×.

3.3. Linking the length scales

At this stage, two different DIC methods for obtaining opening (and closure) load levels independently from macroscale and microscale experimentation have been described. Crack closure levels calculated from the macroscale full-field effective K method are shown as horizontal lines in Fig. 7 where they are compared to the microscale displacement gage results. Since the opening and closure values obtained through the macroscale method were very close to each other (due to the small

Author's personal copy

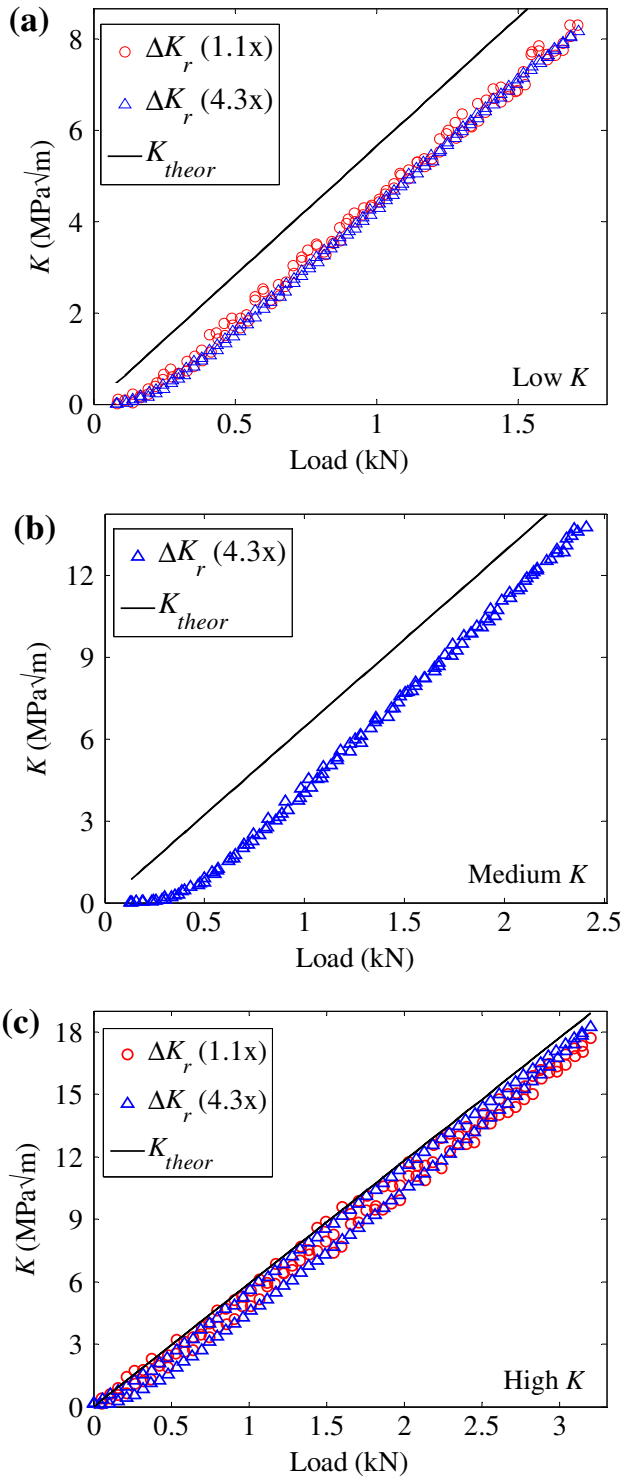

Fig. 12. *K* versus load plots for the: (a) low *K*, (b) medium *K*, and (c) high *K* experiments. Results from two magnifications are shown (1.1× magnification images were not obtained for the medium *K* experiment).

hystereses in the ΔK_r versus load curves) the lines shown in Fig. 7 are average values that represent both opening and closure levels well. The opening/closure levels computed with the full-field effective *K* method are 14%, 15%, and 5% of peak load for the low, medium, and high *K* experiments, respectively. For the low *K* experiment, full-field effective *K* closure levels agree with displacement gages far from the tip (in the region of constant opening level). The effective *K* method gives a measure of local crack opening far from the tip in the plateau region. If this value is known, it is believed that a measure of crack tip opening load could be estimated from full-field measurements. It appears from Fig. 7 that a similar agreement between the two methods is likely for the medium and high *K* experiments as well. Note, however, that in all three experiments, closure levels from the full-field effective *K* method are lower than almost all displacement gage measurements. Consequently,

Author's personal copy

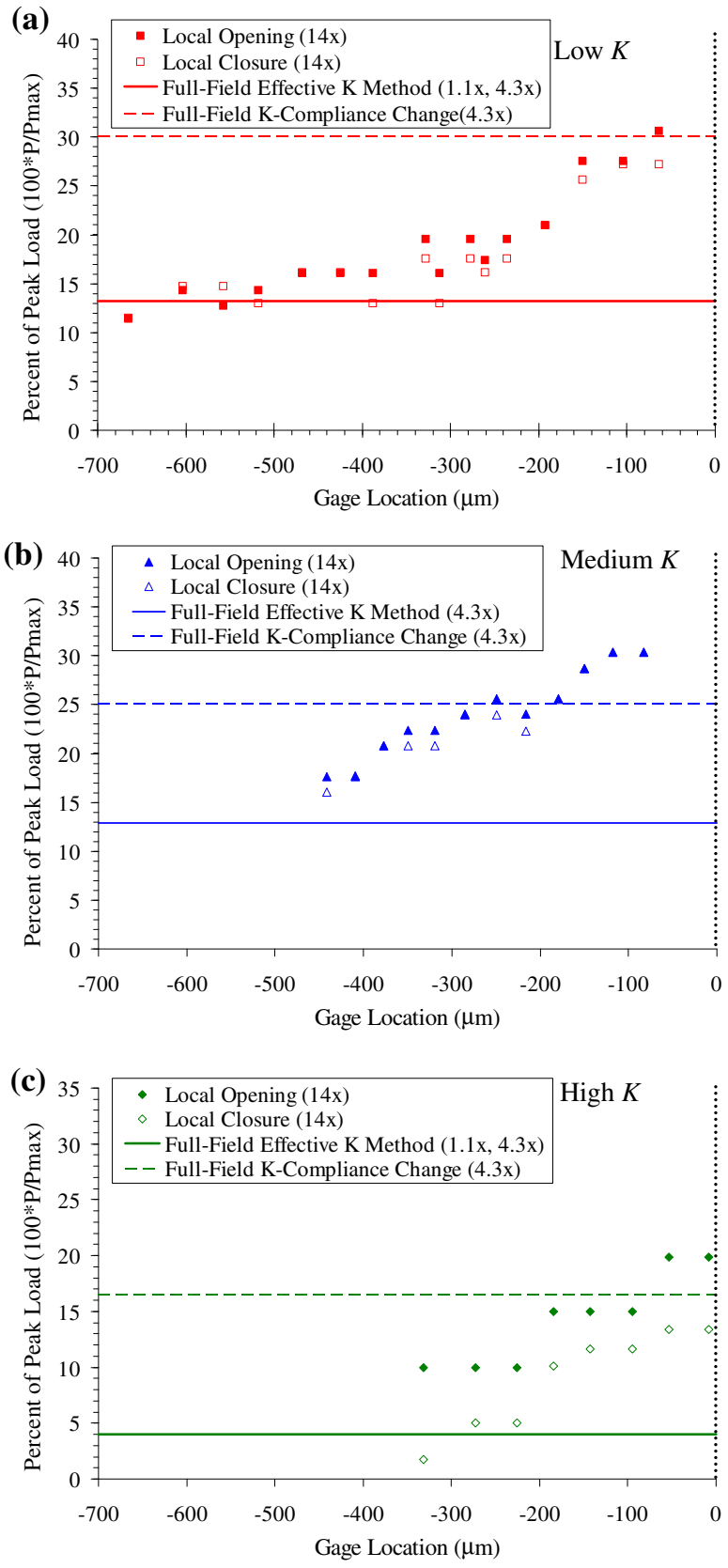

Fig. 13. Crack opening levels from the full-field *K*-compliance method along with results from the full-field effective *K* method and local displacement gage results for comparison: (a) low *K*, (b) medium *K*, (c) high *K*. The horizontal axis represents gage distance behind the crack tip. The vertical axis represents the percentage of the opening (or closure) load, *P*, divided by the peak load, P_{max}.

the full-field effective *K* method is more conservative since it would lead to a higher crack growth rate by the modified Paris relationship (2).

Author's personal copy

As mentioned earlier, the regression value of K is essentially a measure of displacement in the specimen, and the ΔK_r versus load curve behaved similarly to the load versus displacement curve (compare Figs. 3 and 11b). Since the slope of the ΔK_r versus load curve is similar to a compliance measurement, Elber's technique of defining crack closure through compliance change can be applied to the ΔK_r versus load plots (Fig. 12) exactly as it was for the load versus displacement plots. The result is a *second full-field method* for measuring crack closure; this method will be referred to as the "full-field K-compliance method". This method was used to estimate crack tip opening levels by adapting the ASTM compliance offset technique to use the (global) load versus K curve instead of the (local) load versus displacement curves of each gage.

The results of this technique performed on the full-field data at 4.3× are compared to results of the other two methods (DIC displacement gages and full-field effective K method) in Fig. 13a–c for the low, medium, and high K experiments, respectively. Crack opening values obtained from the full-field K-compliance method (at 4.3×) appear to be slightly lower than crack opening levels predicted by an extrapolation of local values for all three experiments. This is in contrast to the full-field effective K method that gives opening levels that are more representative of local values far from the crack tip. Analyzing the full-field 4.3× displacement field as if it was a displacement gage gives results that represent an average of the local opening levels within the imaged region. Thus, the full-field K-compliance method can be thought of in some sense as providing average local crack opening levels using a larger, full-field displacement gage.

4. Conclusions

Two full-field DIC methods for measuring crack closure levels during fatigue crack growth in Ti were introduced and compared to a DIC based displacement gage method. Including the T-stress term in the least squares regression was necessary for reliable results from the full-field techniques. Results from the three techniques were compared for low, medium and high K experiments (with maximum K values of 9.7 MPa$\sqrt{}$m (with $R = 0.05$), 15.4 MPa$\sqrt{}$m (with $R = 0.05$), and 18.9 MPa$\sqrt{}$m (with $R \approx 0$), respectively). Crack opening levels calculated from the full-field effective K method agree with displacement gage closure levels far from the crack tip in the constant opening level region. The second full-field method, the full-field K-compliance method, gives crack opening levels that are an average of local values over the correlated region. The use of these full-field methods would allow effective stress intensity factors to be measured on a full-field basis circumventing some of the drawbacks of placing displacement gages in contact with the sample near the crack tip.

A comparison of the low and medium K experiments indicates there could be some small influence of the maximum stress intensity factor as described in [25]; however, the current experiments are inconclusive in this regard. The ratio of fatigue crack length to notch length was found to affect crack closure levels, confirming the results of Sehitoglu [6]. Displacement gage measurements of crack tip closure levels (35% and 34% for low and medium K experiments) agree with the limited published values for this material (27–42%).

At this time, it is unclear how to predict crack growth rates from the full-field measurements of crack closure presented here. An extensive testing program could help shed light on this issue but is beyond the scope of this paper. Our focus here is to introduce full-field crack closure measurement techniques and to use a multiscale experimental approach to compare closure levels obtained through microscale and macroscale experiments on the same sample. The full-field crack closure techniques demonstrated here use lower magnification images than the DIC displacement gage technique (in this case, 1.1× compared to 14×). Since high quality, high magnification images for DIC can be difficult to obtain, these full-field techniques could be a valuable, easier method for estimating closure levels. This could be of great use in many engineering applications where obtaining approximate answers with less effort is desired.

Acknowledgements

This work was supported by the Midwest Structural Sciences Center (MSSC). The MSSC is supported by the U.S. Air Force Research Laboratory Air Vehicles Directorate under contract number FA8650-06-2-3620. Computer programs for synchronizing the load frame with the camera were provided by Rick Rottet of the Advanced Materials Testing and Evaluation Laboratory at the University of Illinois at Urbana-Champaign.

References

[1] Paris P, Erdogan F. A critical analysis of crack propagation laws. Basic Engng Trans ASME Series D 1963;85:528–34.
[2] McEvily AJ, Boettner RC. On fatigue crack propagation in FCC metals. Acta Metallurgica 1963;11:725–43.
[3] Elber W. The significance of fatigue crack closure. ASTM – STP 486; 1971. p. 230–42.
[4] Elber W. Fatigue crack closure under cyclic tension. Engng Fracture Mech 1970;2:37–45.
[5] Sehitoglu H. Characterization of crack closure. ASTM – STP 868; 1983. p. 361–80.
[6] Sehitoglu H. Crack opening and closure in fatigue. Engng Fracture Mech 1985;21(2):329–39.
[7] Schijve J. Fatigue crack closure: observations and technical significance. ASTM – STP 982; 1988. p. 5–34.
[8] Allison JE, Ku RC, Pompetzki MA. A comparison of measurement methods and numerical procedures for the experimental characterization of fatigue crack closure. ASTM – STP 982; 1988. p. 171–85.
[9] Macha DE, Corbly DM, Jones JW. On the Variation of fatigue-crack-opening load with measurement location. Exp Mech 1979;19(6):207–13.
[10] Riddell WT, Piascik RS, Sutton MA, Zhao W, McNeill SR, Helm JD. Determining fatigue crack opening loads from near-crack-tip displacement measurements. ASTM – STP 1343; 1999. p. 157–74.
[11] Sutton MA, Zhao W, McNeill SR, Helm JD, Piascik RS, Riddell WT. Local crack closure measurements: development of a measurement system using computer vision and a far-field microscope. ASTM – STP 1343; 1999. p. 145–56.

Author's personal copy

[12] Sutton MA, Wolters WJ, Peters WH, Ranson WF, Mcneil SR. Determination of displacements using an improved digital image correlation method. Image Vision Comput 1983;1(3):133–9.
[13] Dally JW, Riley WF. Experimental stress analysis. 4th ed. Knoxville TN: College House Enterprises LLC; 2005. chapter 19.
[14] Donald K, Paris PC. An evaluation of ΔK_{eff} estimation procedures on 6061-T6 and 2024-T3 aluminum alloys. Int J Fatigue 1999;21:S47–57.
[15] Paris PC, Tada H, Donald JK. Service load fatigue damage – a historical perspective. Int J Fatigue 1999;21:S35–46.
[16] Paris PC, Lados D, Tada H. Reflections on identifying the real ΔK_{eff} in the threshold region and beyond. Engng Fracture Mech 2008;75:299–305.
[17] Chermahini RG, Shivakumar KN, Newman Jr JC, Blom AF. Three-dimensional aspects of plasticity-induced fatigue crack closure. Engng Fracture Mech 1989;34(2):393–401.
[18] Budiansky B, Hutchinson JW. Analysis of closure in fatigue crack growth. J Appl Mech 1978;45:267–76.
[19] Lalor PL, Sehitoglu H. Fatigue crack closure outside a small-scale yielding regime. ASTM – STP 982; 1987. p. 342–60.
[20] Fleck NA, Newman JC Jr. Analysis of crack closure under plane strain conditions. ASTM – STP 982; 1988. p. 319–41.
[21] Sehitoglu H, Sun W. Modeling of plane strain fatigue crack closure. J Engng Mater Tech 1991;113:31–40.
[22] Suresh S, Ritchie RO. Near-threshold fatigue crack propagation: a perspective on the role of crack closure. In: Davidson D, Suresh S, editors. Fatigue crack growth threshold concepts. The Metallurgical Society of AIME; 1984. p. 227–61.
[23] Abanto-Bueno J, Lambros J. Experimental determination of cohesive failure properties of a photodegradable copolymer. Exp Mech 2005;45(2):144–52.
[24] ASTM Standard E647-05 Standard test method for measurement of fatigue crack growth rates. ASTM International; 2005.
[25] Shih TT, Wei RP. A study of crack closure in fatigue. Engng Fracture Mech 1974;6:19–32.
[26] Takao K, Matsumoto K, Nisitani H. Fatigue crack closure in commercially pure titanium (measurement using DC-potential drop method). Nippon Kikai Gakkai Ronbunshu A Hen/Trans of Japan Society of Mechanical Engineers 1985;51(462):450–4.
[27] Tada H, Paris PC, Irwin GR. The stress analysis of cracks handbook. 2nd ed. St. Louis MO: Paris Productions Inc.; 1985.
[28] Williams ML. On the stress distribution at the base of a stationary crack. J Appl Mech 1957;24:109–14.
[29] Kmiec KJ. Determination of the Fracture Parameters Associated with Mixed Mode Displacement Fields and Applications of High Density Geometric Moire. M.S. Thesis Texas A&M University; 1994.
[30] Leevers PS, Radon JC. Inherent stress biaxiality in various fracture specimen geometries. Int J Fracture 1982;19:311–25.
[31] McNeill SR, Peters WH, Sutton MA. Estimation of stress intensity factor by digital image correlation. Engng Fracture Mech 1987;28(1):101–12.
[32] Abanto-Bueno J, Lambros J. Parameters controlling fracture resistance in functionally graded materials under mode I loading. Int J Solids Struct 2006;43(13):3920–39.